Constraining ALPs with Hard X-Ray Emission from Magnetars

Kuver Sinha
University of Oklahoma

Based on arXiv:1804.01992
with Jean-Francois Fortin

Axion-like-Particles (ALPs)

ALPs: strong CP problem, string axiverse, etc.

Detection typically relies on ALP couplings:

$$\mathcal{L} \supset -\frac{g}{4} a F_{\mu\nu} \tilde{F}^{\mu\nu} + g_{aN} (\partial_\mu a) \bar{N} \gamma^\mu \gamma_5 N$$

Strong magnetic fields are especially useful

Magnetars have the strongest magnetic fields

Also lots of data

Helioscope

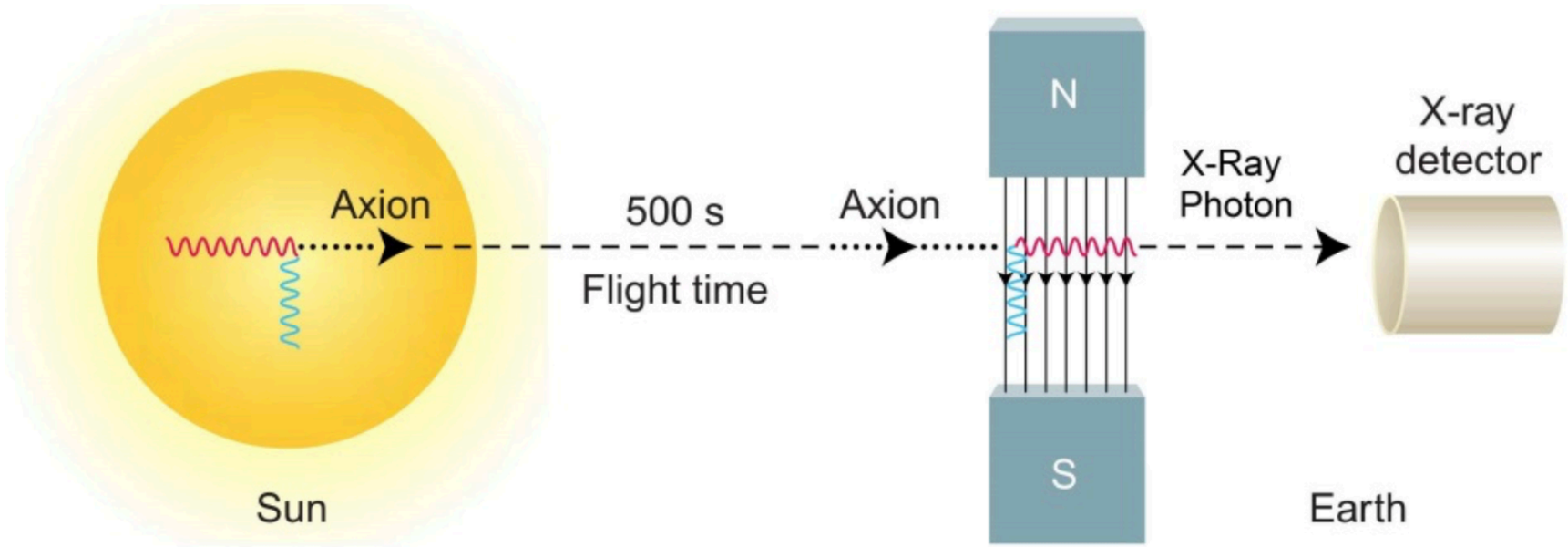

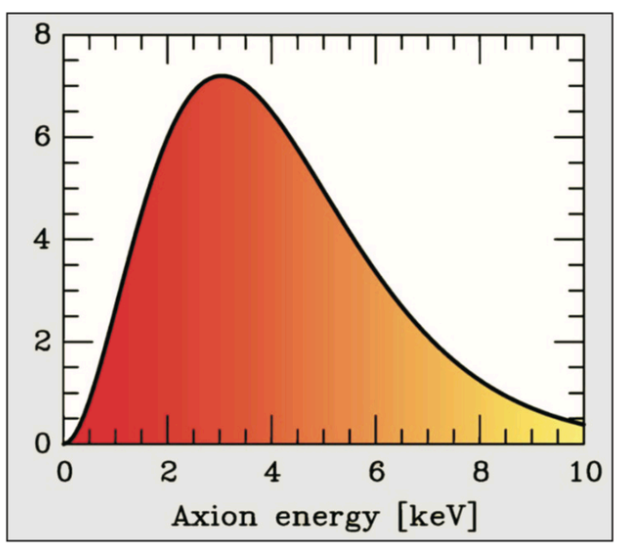

$$\mathcal{L} \supset -\frac{g}{4} a F_{\mu\nu} \tilde{F}^{\mu\nu}$$

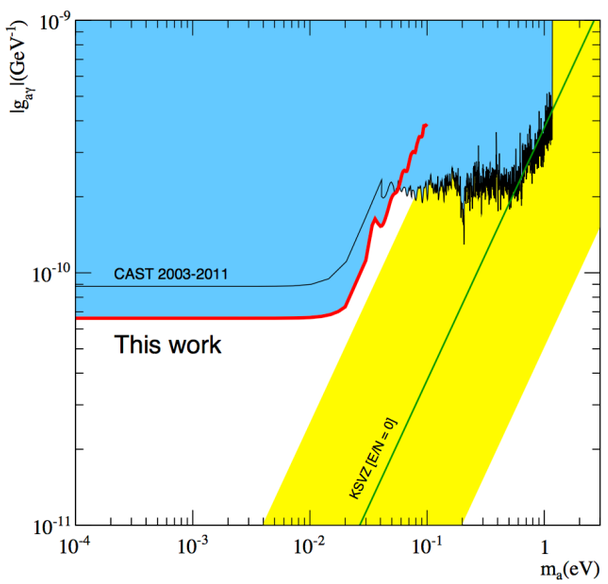

CAST (2017)

Main Idea

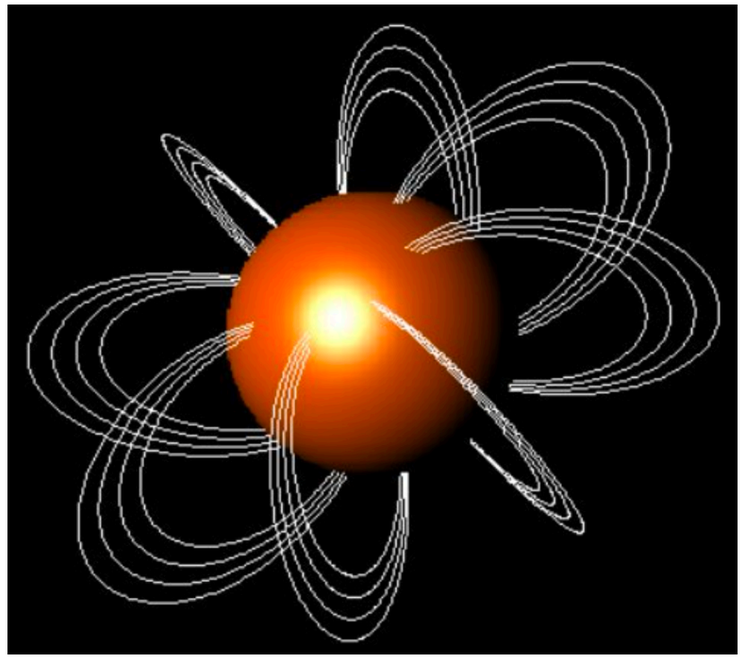

$$B_0 = 20 \times 10^{14}\,\mathrm{G}$$

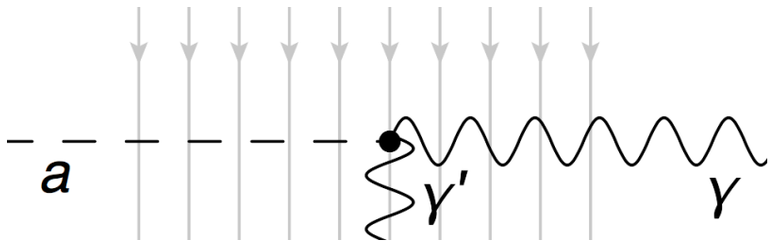

$$B = B_0 (r_0/r)^3$$

integral

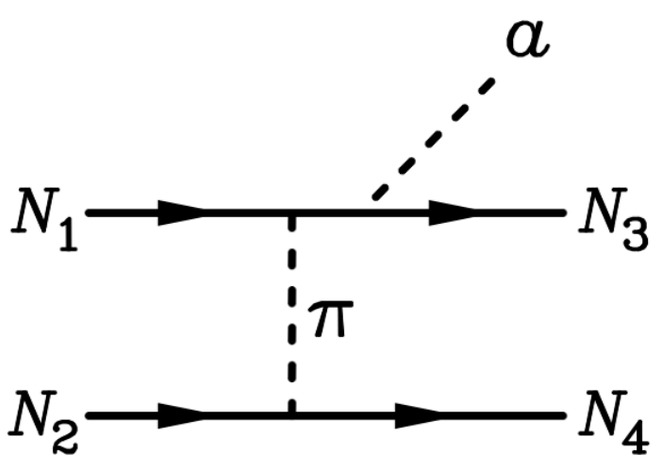

Hard X-rays

Soft X-rays **Heyl/Lai (2006)**

Perna et. al. (2012)

Radio Waves

Pshirkov/Popov (2007)

ALP Wave Equation

$\mathbf{E}, a \propto e^{i\omega t}$

photon wavelength much smaller than magnetar radius

linearized wave equation

$$i\frac{d}{dr}\begin{pmatrix} a \\ E_\parallel \end{pmatrix} = \begin{pmatrix} \omega + \Delta_a & \Delta_M \\ \Delta_M & \omega + \Delta_\parallel \end{pmatrix}\begin{pmatrix} a \\ E_\parallel \end{pmatrix}$$

Raffelt/Stodolsky (1988)

axion mass term $\Delta_a = -\frac{m_a^2}{2\omega}$

mixing term $\Delta_M = \frac{1}{2} g B \sin\theta$

Euler-Heisenberg term $\Delta_\parallel = \frac{1}{2} q \omega \sin^2\theta$ $q = \frac{7\alpha}{45\pi} b^2 \hat{q}$ $\hat{q} = \frac{1+1.2b}{1+1.33b+0.56b^2}$

Schwinger (1951), Adler (1971), Heyl/Hernquist (2010)

magnetic field $b = B/B_Q$

$B_Q = m_e^2 c^3/(e\hbar) = 4.414\times10^{13}$ G

Mixing Angle

$$i\frac{d}{dx}\begin{pmatrix} a \\ E_\parallel \end{pmatrix} = \begin{pmatrix} \omega r_0 + \Delta_a r_0 & \Delta_M r_0 \\ \Delta_M r_0 & \omega r_0 + \Delta_\parallel r_0 \end{pmatrix}\begin{pmatrix} a \\ E_\parallel \end{pmatrix} = \begin{pmatrix} A(x) & D(x) \\ D(x) & B(x) \end{pmatrix}\begin{pmatrix} a \\ E_\parallel \end{pmatrix}$$

Mixing angle: $\frac{1}{2}\tan 2\theta = \dfrac{D(x)}{B(x) - A(x)}$

$\omega = 100\,\mathrm{keV},\ m_a = 10^{-8}\,\mathrm{keV},$
$r_0 = 10\,\mathrm{km},\ B_0 = 20\times 10^{14}\,\mathrm{G}$
$g = 10^{-15}\,\mathrm{keV}^{-1}.$

$$D(x) = \Delta_M r_0 = \frac{\Delta_{M0} r_0}{x^3} \approx \frac{3.0\times 10^5}{x^3}$$

$$B(x) = \frac{\Delta_{\parallel 0}\hat{q}(x)}{x^6}\, r_0 \approx \frac{8.6\times 10^{13}}{x^6} \qquad A(x) \approx \Delta_a r_0 \approx -2.5\times 10^{-5}$$

Impossible?

nitude. Although in a detailed calculation of the axion-photon conversion rates the inhomogeneity of the field must be properly included as in our perturbative solution Eq. (33), it is clear that the conversion is now dramatically suppressed due to the magnetically induced vacuum index of refraction. Given this suppression it is difficult to imagine the occurrence of *observable* effects.[36]

Raffelt/Stodolsky (1988)

Solution: n-body

general n-body oscillation problem

$$i\frac{da_i(x)}{dx} = \sum_{j=1}^{n} A_{ij}(x)a_j(x)$$

$$A^*_{ji}(x) = A_{ij}(x) \qquad \frac{d}{dx}\sum_{i=1}^{n}|a_i(x)|^2 = 0$$

$$a_i(x) = \left\{\prod_{j=i}^{n-1}\sin[\chi_j(x)]\right\}\cos[\chi_{i-1}(x)]e^{-i\phi_i(x)}$$

$$\frac{d\chi_{i-1}(x)}{dx} = \sum_{j=1}^{n} A_{ij}(x)S_{ij}(x) + \cot[\chi_{i-1}(x)]\sum_{j=i+1}^{n}\left\{\sum_{\ell=1}^{n} A_{j\ell}(x)S_{j\ell}(x)\right\}\cot[\chi_{j-1}(x)]\left\{\prod_{k=i}^{j-2}\csc^2[\chi_k(x)]\right\}$$

$$\frac{d\phi_i(x)}{dx} = \sum_{j=1}^{n} A_{ij}(x)C_{ij}(x)$$

coefficients

$$S_{ij}(x) = \frac{\left\{\prod_{k=j}^{n-1}\sin[\chi_k(x)]\right\}\cos[\chi_{j-1}(x)]}{\left\{\prod_{k=i}^{n-1}\sin[\chi_k(x)]\right\}\sin[\chi_{i-1}(x)]}\sin[\phi_j(x)-\phi_i(x)],$$

$$C_{ij}(x) = \frac{\left\{\prod_{k=j}^{n-1}\sin[\chi_k(x)]\right\}\cos[\chi_{j-1}(x)]}{\left\{\prod_{k=i}^{n-1}\sin[\chi_k(x)]\right\}\cos[\chi_{i-1}(x)]}\cos[\phi_j(x)-\phi_i(x)].$$

Solution: 2-body

$$i\frac{d}{dx}\begin{pmatrix} a \\ E_\parallel \end{pmatrix} = \begin{pmatrix} \omega r_0 + \Delta_a r_0 & \Delta_M r_0 \\ \Delta_M r_0 & \omega r_0 + \Delta_\parallel r_0 \end{pmatrix}\begin{pmatrix} a \\ E_\parallel \end{pmatrix} = \begin{pmatrix} A(x) & D(x) \\ D(x) & B(x) \end{pmatrix}\begin{pmatrix} a \\ E_\parallel \end{pmatrix}$$

$$a(x) = \cos[\chi(x)]e^{-i\phi_a(x)}$$

$$E_\parallel(x) = i\sin[\chi(x)]e^{-i\phi_E(x)}$$

$$\frac{d\chi(x)}{dx} + i\cot[\chi(x)]\left[\frac{d\phi_a(x)}{dx} - A(x)\right] = -D(x)e^{i[\phi_a(x)-\phi_E(x)]},$$
$$\frac{d\chi(x)}{dx} - i\tan[\chi(x)]\left[\frac{d\phi_E(x)}{dx} - B(x)\right] = -D(x)e^{-i[\phi_a(x)-\phi_E(x)]}$$

$$\frac{d\chi(x)}{dx} = -D(x)\cos[\Delta\phi(x)],$$
$$\frac{d\Delta\phi(x)}{dx} = A(x) - B(x) + 2D(x)\cot[2\chi(x)]\sin[\Delta\phi(x)]$$

Conversion Probability

$$P_{a\to\gamma}(x) = \sin^2[\chi(x)]$$

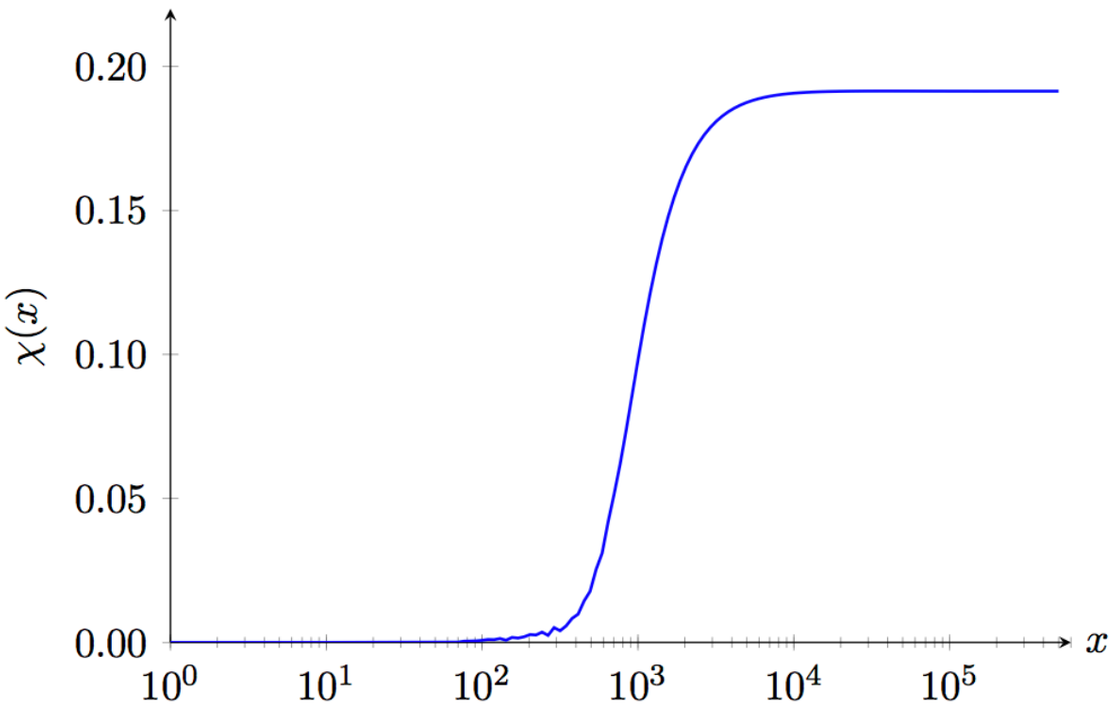

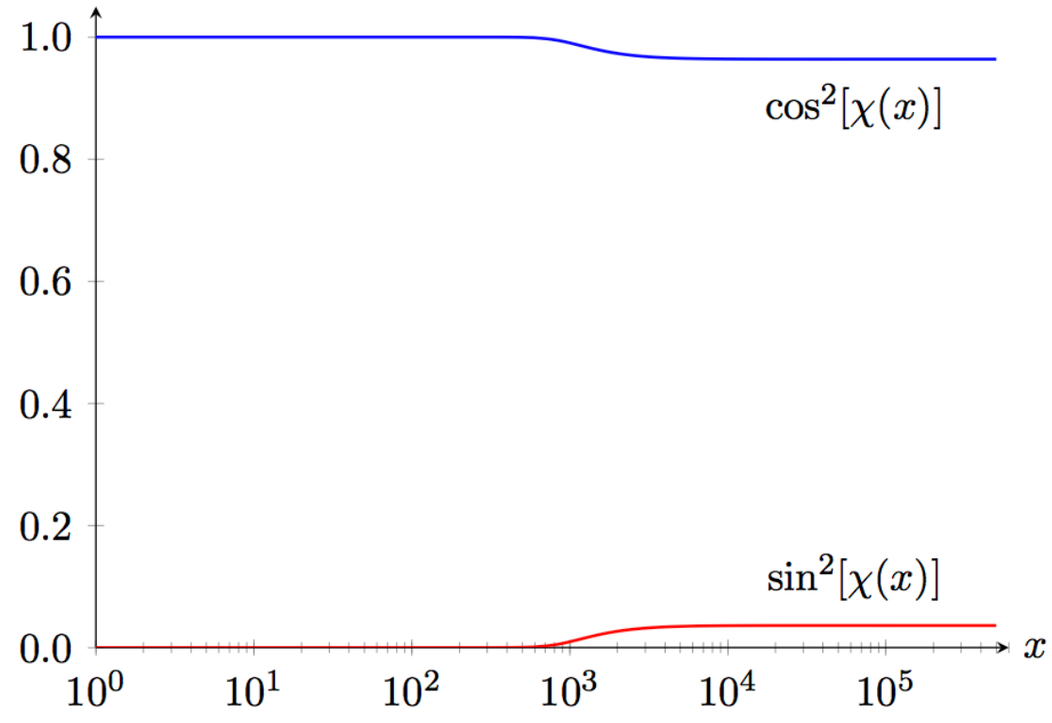

$$\omega = 100\,\mathrm{keV},\ m_a = 10^{-8}\,\mathrm{keV},\ g = 10^{-15}\,\mathrm{keV}^{-1},\ r_0 = 10\,\mathrm{km},\ B_0 = 20\times10^{14}\,\mathrm{G}$$

Probability Dependences

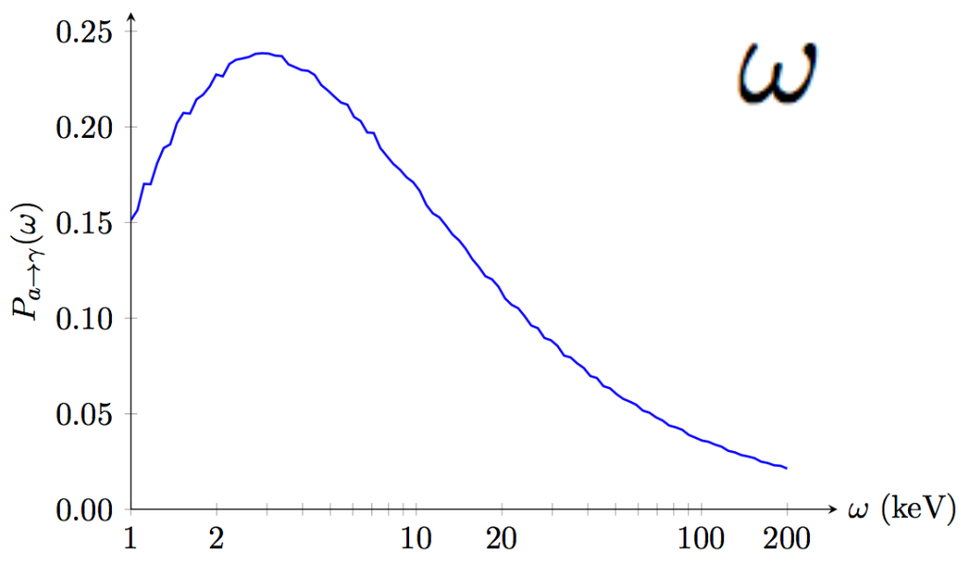

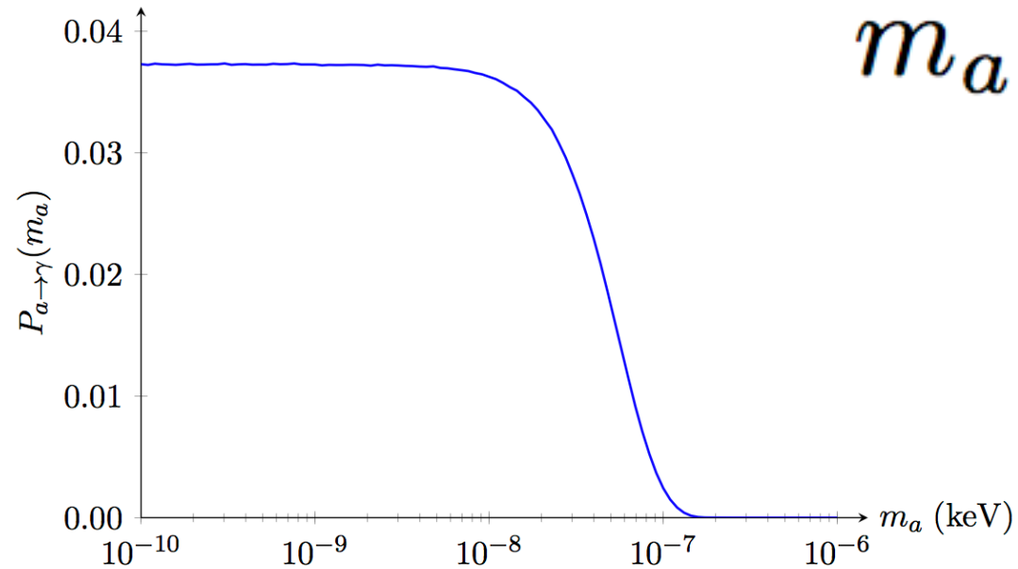

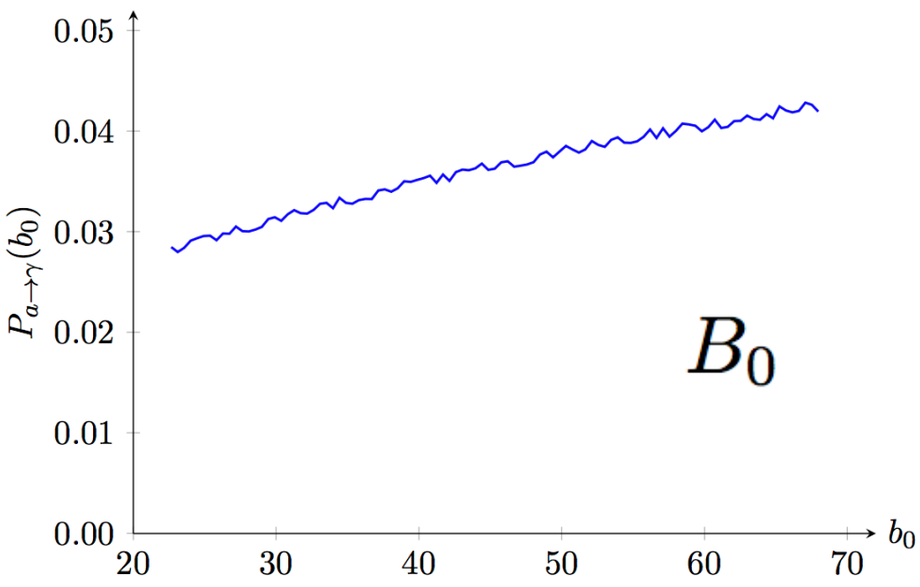

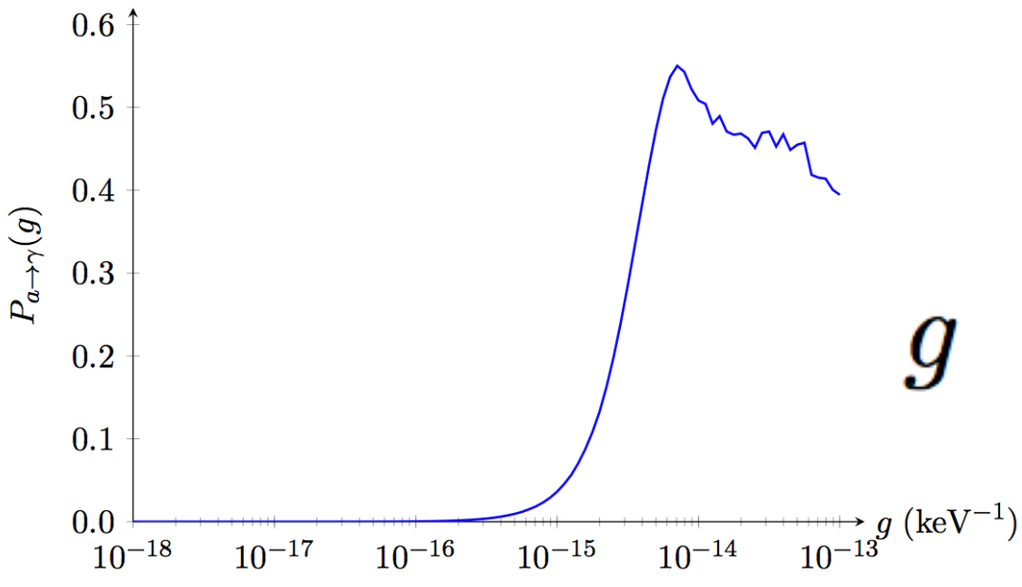

$$\omega = 100\,\mathrm{keV},\ m_a = 10^{-8}\,\mathrm{keV},\ g = 10^{-15}\,\mathrm{keV}^{-1},\ r_0 = 10\,\mathrm{km},\ B_0 = 20\times10^{14}\,\mathrm{G}$$

Parameter Scan

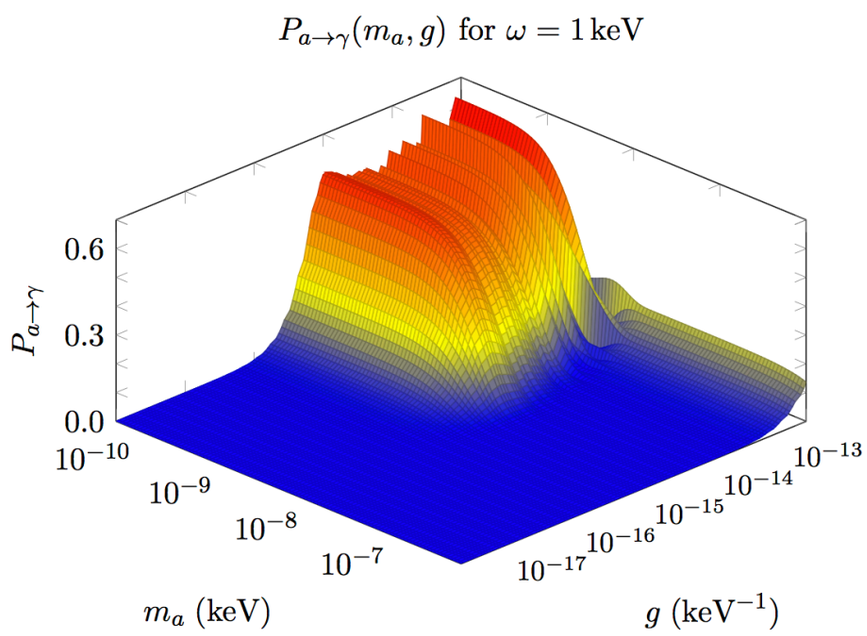

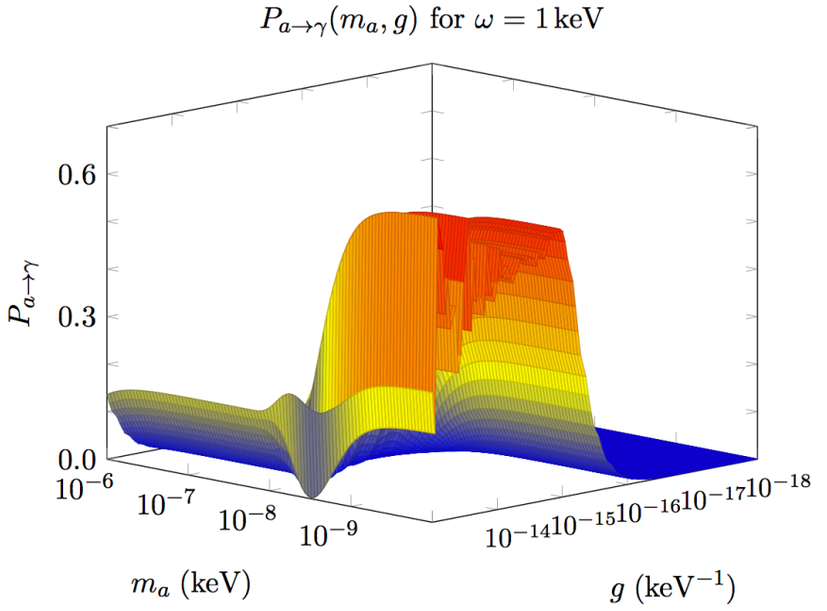

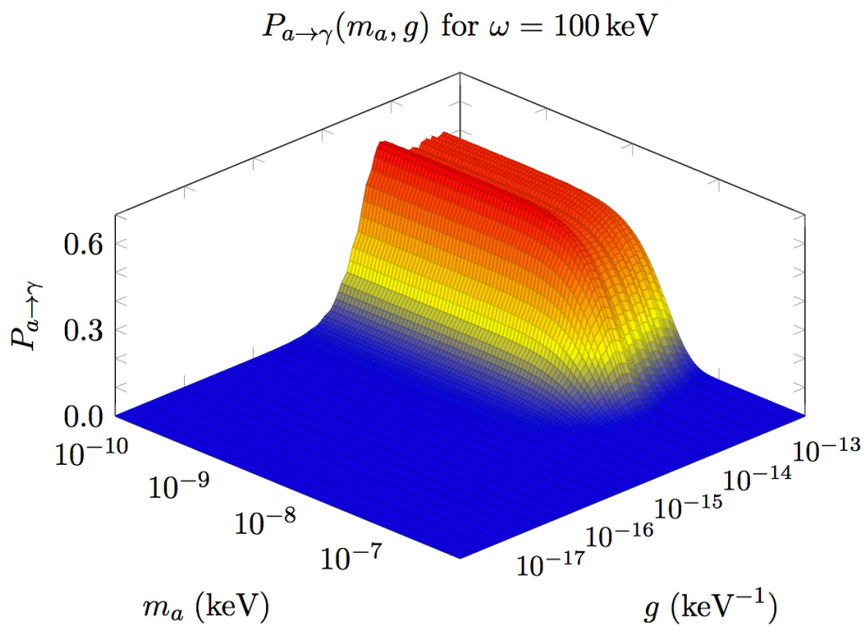

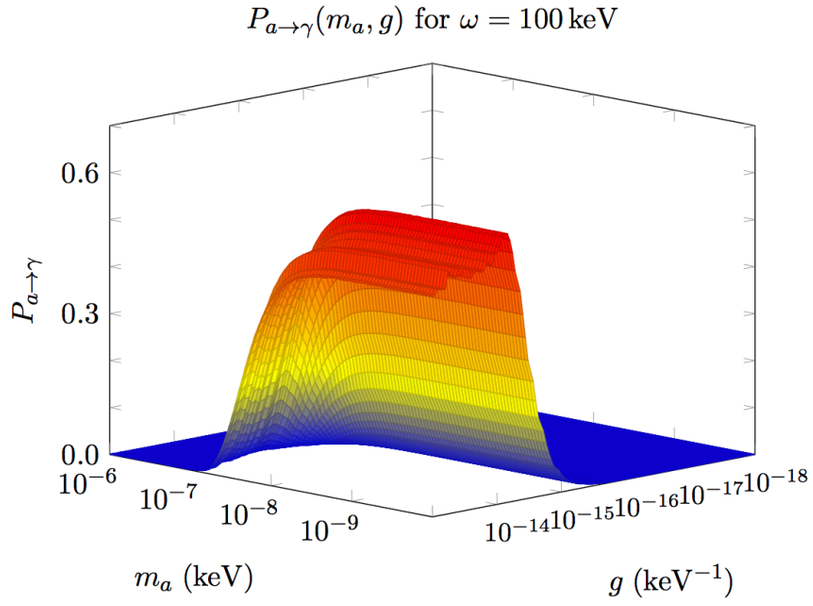

ALP Production

agnostic: just subdominant to neutrino cooling

Sedrakian (2017), Balantekin et. al. (2017),…

$$L_{a\to\gamma} = \frac{N_a}{2\pi}\int_0^{2\pi} d\theta \int_{\omega_i}^{\omega_f} d\omega\, \omega \frac{dN_a}{d\omega} P_{a\to\gamma}(\omega,\theta)$$

$$\frac{1}{2\pi}\int_0^{2\pi} d\theta\, P_{a\to\gamma}(\omega,\theta) \to R_\theta P_{a\to\gamma}(\omega,\pi/2)$$

$$R_\theta = 0.6$$

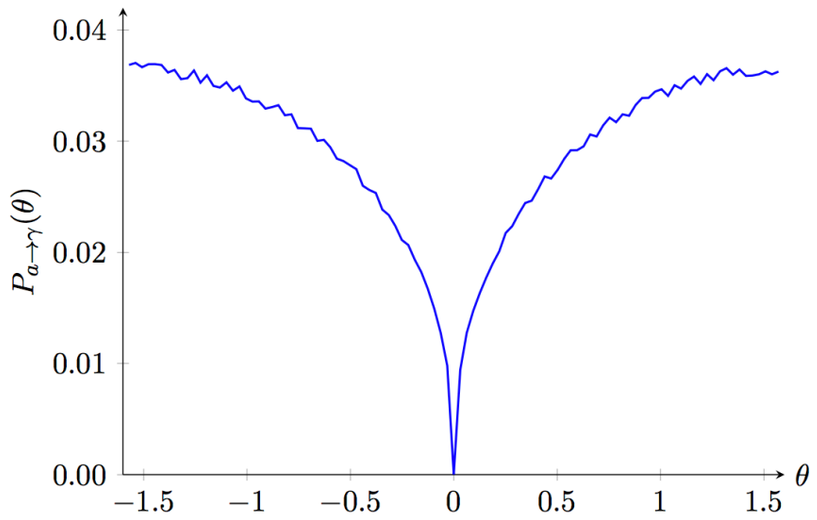

$$L_a = N_a \int_0^{\infty} d\omega\, \omega \frac{dN_a}{d\omega} \leq L_\nu = 4\pi \int_0^{r_0} dr\, r^2 \dot{q}_\nu$$

ALP Production

$$N_a \leq \frac{4\pi r_0^3 \dot{q}_\nu}{3\int_0^\infty d\omega\, \omega \frac{dN_a}{d\omega}}$$

$$L_{a\to\gamma} = \frac{4\pi r_0^3 \dot{q}_\nu R_\theta}{3\int_0^\infty d\omega\, \omega \frac{dN_a}{d\omega}} \int_{\omega_i}^{\omega_f} d\omega\, \omega \frac{dN_a}{d\omega} P_{a\to\gamma}(\omega, \pi/2)$$

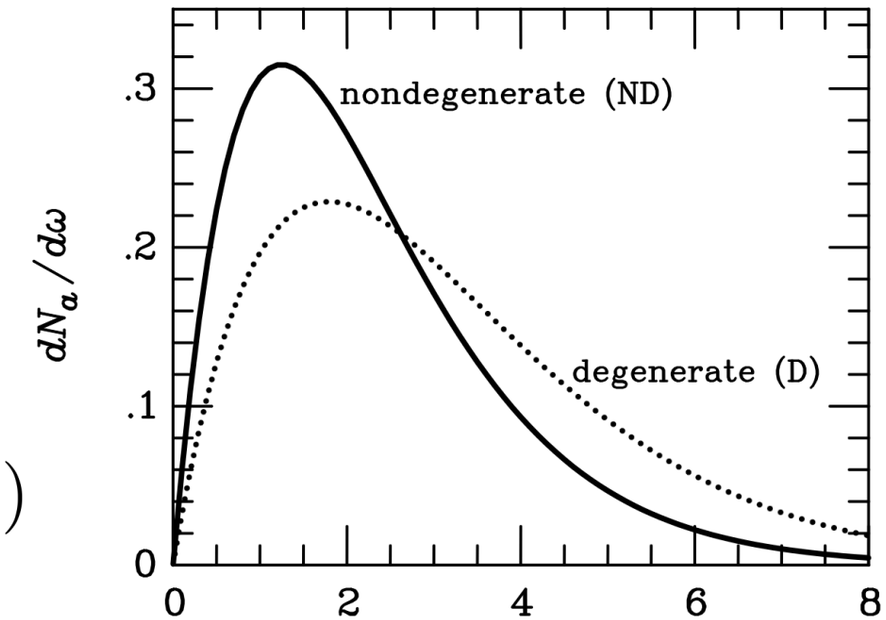

$$\frac{dN_a}{d\omega} = \frac{x^2(x^2+4\pi^2)e^{-x}}{8(\pi^2\zeta_3 + 3\zeta_5)(1-e^{-x})}$$

$$\int_0^\infty d\omega\, dN_a/d\omega = 1$$

$$x = \omega/k_B T$$

Iwamoto (1984)
Brinkmann/Turner (1988)
Raffelt (1996)

modified Urca production

$$\dot{q}_\nu = (7\times 10^{20}\,\mathrm{erg}\cdot\mathrm{s}^{-1}\cdot\mathrm{cm}^{-3}) \left(\frac{\rho}{\rho_0}\right)^{2/3} R_M \left(\frac{T}{10^9\,\mathrm{K}}\right)^8$$

$\rho_0 = 2.8\times 10^{14}\,\mathrm{g}\cdot\mathrm{cm}^{-3}$ is the nuclear saturation density

Neutrino Cooling

direct Urca

$$\dot{q}_\nu^D \sim 10^{27}\, T_9^6\, \mathcal{R}_D\, \mathrm{erg\ s^{-1}\ cm^{-3}}\ (\rho \gtrsim 10^{15}\, \mathrm{g\ cm^{-3}}),$$

modified Urca

$$\dot{q}_\nu^M \sim 7 \times 10^{20}\, T_9^8 \left(\frac{\rho}{\rho_{\rm nuc}}\right)^{2/3} \mathcal{R}_M\, \mathrm{erg\ s^{-1}\ cm^{-3}},$$

Cooper pair cooling

$$\dot{q}_\nu^{CP} \sim 10^{21} \left(\frac{\rho}{\rho_{\rm nuc}}\right)^{1/3} T_9^7\, f\left(\frac{T_{\rm core}}{T_{\rm crit}}\right) \mathrm{erg\ s^{-1}\ cm^{-3}},$$

Beloborodov (2017)

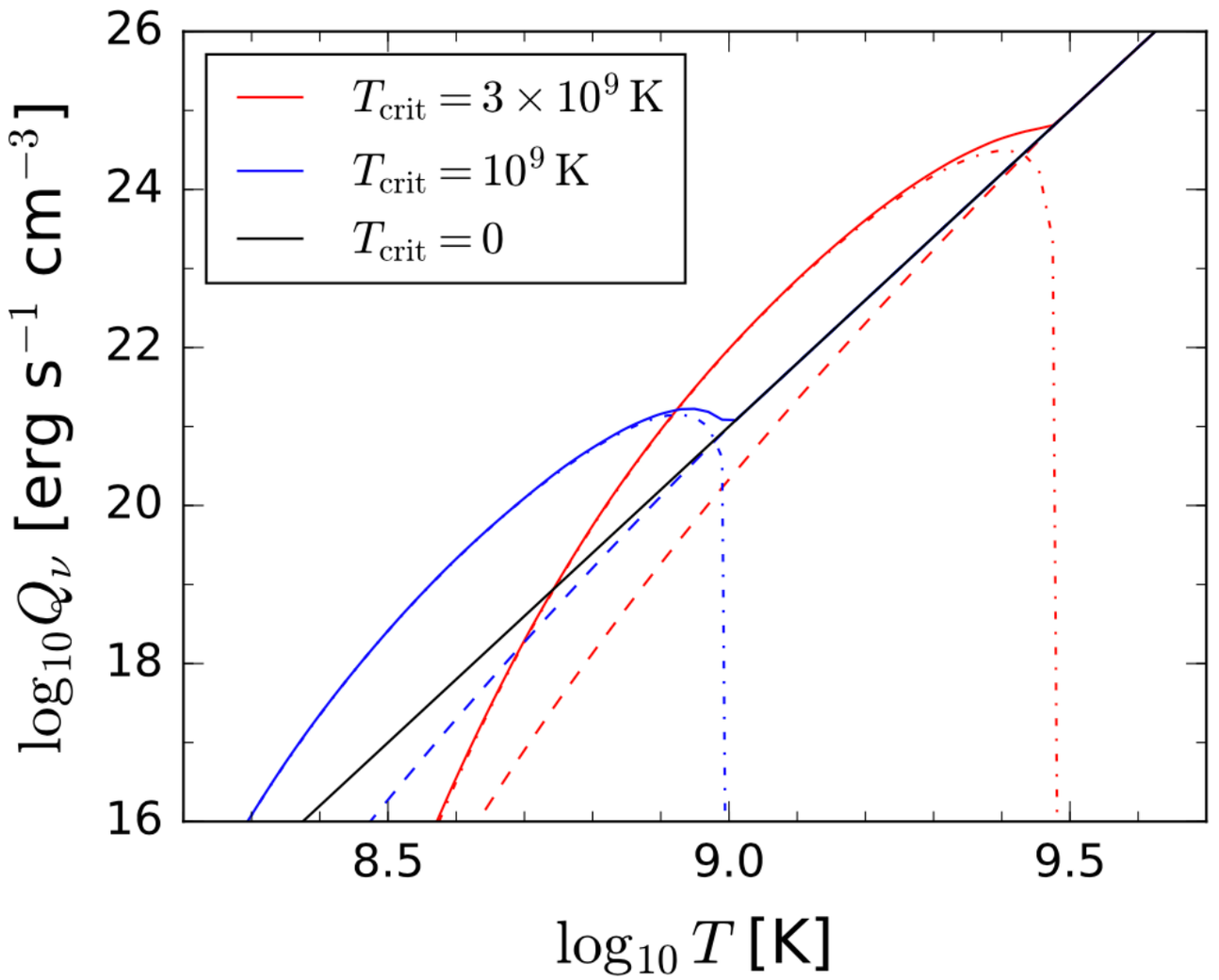

Figure 2. Neutrino cooling rate as a function of temperature in the core at density $\rho_{\rm nuc} = 2.8 \times 10^{14}$ g cm^{-3}. The black curve shows Murca cooling assuming no superfluidity ($T_{\rm crit} < 10^8$ K). The colored curves show the cooling of matter with non-superfluid protons and superfluid neutrons, for two cases: $T_{\rm crit} = 10^9$ K (blue curves) and $T_{\rm crit} = 3 \times 10^9$ K (red curves). The dashed curve shows the Murca contribution, and the dashed–dotted curve shows the Cooper pair contribution; the net cooling rate is shown by the solid curve. A triplet-state neutron pairing is assumed (model B in Yakovlev et al. 2001).

ALP Production

$$\dot{q}_\nu = (7 \times 10^{20}\,\mathrm{erg \cdot s^{-1} \cdot cm^{-3}}) \left(\frac{\rho}{\rho_0}\right)^{2/3} R_M \left(\frac{T}{10^9\,\mathrm{K}}\right)^8$$

$$\dot{q}_a = (1.3 \times 10^{25}\,\mathrm{erg \cdot s^{-1} \cdot cm^{-3}}) \left(\frac{g_{aN}}{10^{-10}\,\mathrm{GeV^{-1}}}\right) \left(\frac{\rho}{\rho_0}\right)^{1/3} \left(\frac{T}{10^9\,\mathrm{K}}\right)^6$$

$$\left(\frac{g^*_{aN}}{10^{-10}\,\mathrm{GeV^{-1}}}\right) = 7.3 \times 10^{-3} \left(\frac{\rho}{\rho_0}\right)^{1/6} \sqrt{R_M} \left(\frac{T}{10^9\,\mathrm{K}}\right)$$

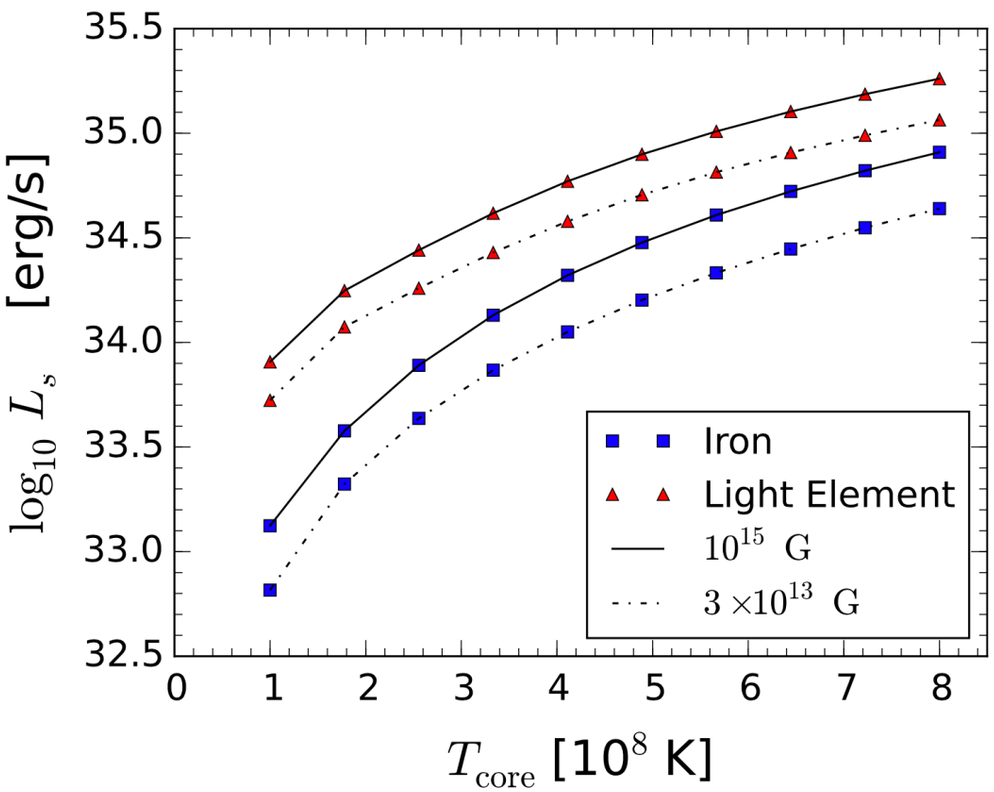

observed at infinity. Each symbol shows a calculated model of steady heat transfer from the core to the stellar surface. The star is assumed to have a dipole magnetic field near the surface, in the heat-blanketing envelope. Two cases are considered: the iron envelope and the maximal light-element envelope, which is called "fully accreted" in Potekhin et al. (2003). The luminosity is shown for two values of the polar magnetic field: $B_p = 3 \times 10^{13}$ G and a more typical one for magnetars $B_p = 10^{15}$ G. As $T_{\rm core}$ approaches 10^9 K, $\mathscr{L}_s^\infty$ approaches the ceiling imposed by neutrino cooling (Potekhin et al. 2007); heating the core to higher temperatures would not significantly increase the surface luminosity.

Beloborodov/Li (2017)

Total Photon Luminosity

$$L_{a\to\gamma} = \frac{4\pi r_0^3 \dot{q}_\nu R_\theta}{3\int_0^\infty d\omega\,\omega\frac{dN_a}{d\omega}} \int_{\omega_i}^{\omega_f} d\omega\,\omega\frac{dN_a}{d\omega} P_{a\to\gamma}(\omega, \pi/2)$$

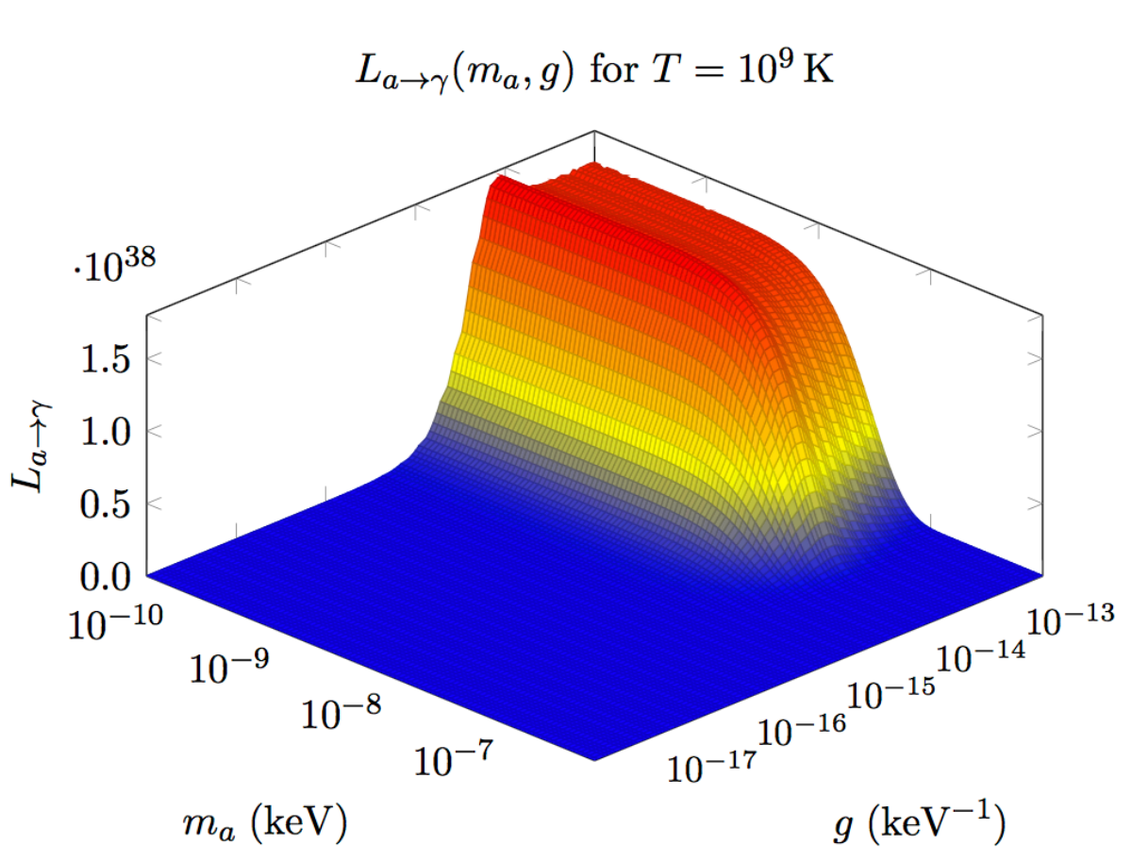

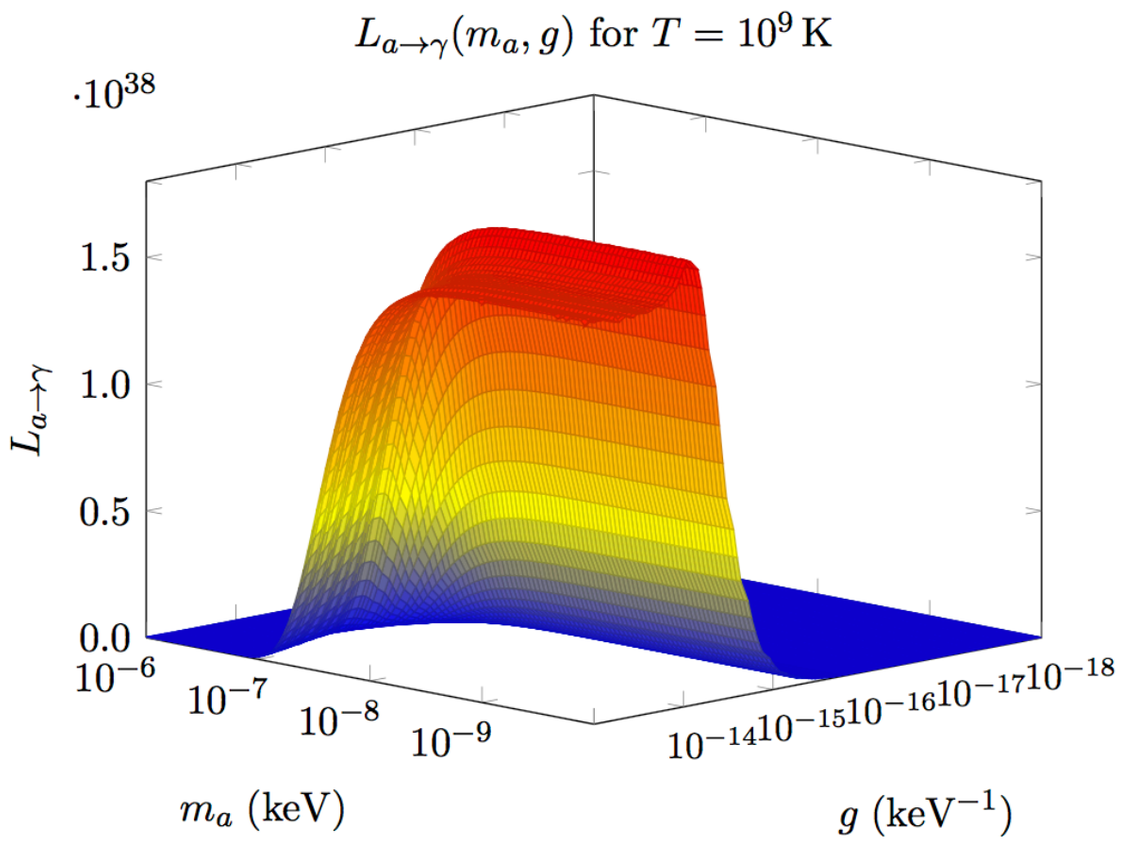

Figure 4. Photon luminosity from ALP-photon oscillations in the broad band from 1 keV to 200 keV in the (m_a, g) plane. The computations are done for SGR 1806-20 assuming $r_0 = 10\,\mathrm{km}$ and $B_0 = 20 \times 10^{14}\,\mathrm{G}$. The magnetar core temperature is assumed to be $T = 10^9\,\mathrm{K}$. The two panels show the same conversion probability from different points of view.

Non-thermal Emission

Besides spectacular outbursts, magnetars produce persistent or decaying X-ray emission with luminosity $L \sim 10^{34} - 10^{36}$ erg s^{-1}. Two peaks are observed in their X-ray spectra, with comparable luminosities. The first peak is near 1 keV; it is associated with thermal emission from the neutron star surface. The second peak is above 100 keV. Its low-energy slope (between 10 and 100 keV) was observed in 7 magnetars[1] (Kuiper et al. 2008; Enoto et al. 2010), with a typical photon index $\Gamma \sim 1 - 1.5$.

Beloborodov (2012)

SGR 1806-20

Name[b]	P (s)	B[c] (10^{14} G)	Age[d] (kyr)	$\dot{E}$[e] 10^{33} erg s^{-1}	D[f] (kpc)	L_X[g] 10^{33} erg s^{-1}	Band[h]
SGR 1806−20	7.55	20	0.24	45	8.7	163 **1200**	OIR/H

Kaspi (2016)

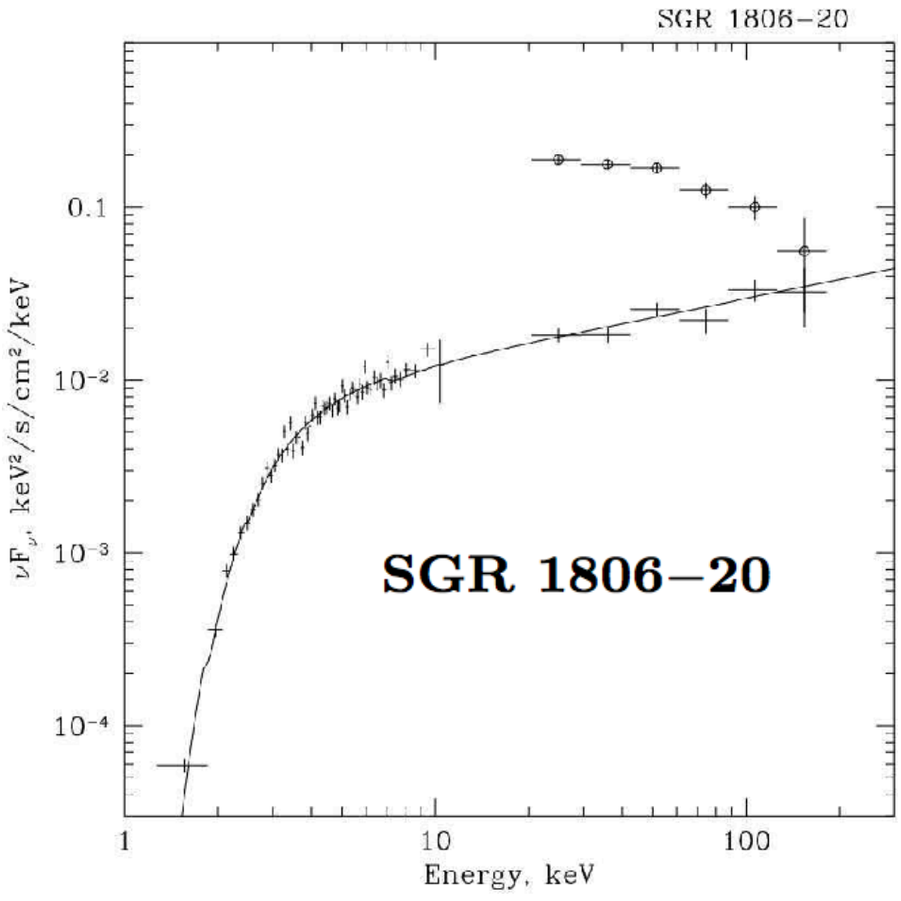

Sunyaev et. al. (2004)

In this letter we present the broad band spectrum (1-200 keV) of the persistent emission of SGR 1806-20 obtory in autumn 2003. The source flux was $\sim 1.3 \times 10^{-10}$ erg s^{-1} cm^{-2}, which corresponds to a source luminosity $\sim 3.6 \times 10^{36}$ erg s^{-1} in this energy band (assuming a source

McGill Online Magnetar Catalog

Table 4: Hard X-ray observations

- This table is available in ASCII and CSV format.
- Back to main catalog.

Name	Cutoff Energy (keV)	PL Index (Pulsed)	Pulsed F_X[a] (10^{-11} erg/s/cm^2)	PL Index (Total)	Total F_X[a] (10^{-11} erg/s/cm^2)	Telescope	Ref.[b]
4U 0142+61	279^{+65}_{-41} [dkh+08]	0.40(15) …	2.68(1.34) …	0.93(6) $0.89^{+0.11}_{-0.10}$	9.09(35) 10.3 [$3.28^{+0.32}_{-0.29}$ (15–60 keV)]	Integral, RXTE Suzaku	[dkh+08] [emn+11]
SGR 0501+4516	>100 [rit+09]	… … …	… … …	0.8(2) … $0.79^{+0.20}_{-0.18}$	… <3.5 [<0.97 (18–60 keV)] $8.4^{+2.0}_{-1.5}$ [$4.8^{+0.8}_{-0.6}$ (20–100 keV)]	Integral Integral Suzaku	[rit+09] [rit+09] [ern+10]
1E 1547.0−5408	>200 [enm+10a]	… $-0.37^{+0.28}_{-0.20}$ $-0.59^{+0.25}_{-0.19}$ $-1.55^{+0.42}_{-0.26}$ … … … … … …	… $6.9^{+1.2}_{-1.0}$ $7.5^{+0.9}_{-1.0}$ 4.1(9) … … … … … …	$1.54^{+0.06}_{-0.05}$ … … … … 1.41(6) 1.45(4) 1.27(11) 1.22(10) 0.87(7)	$17.4^{+1.4}_{-1.8}$ [$12.5^{+0.8}_{-1.1}$ (20–100 keV)] … … … <1.5 25.2(3.7) 18.5(1.8) 21.5(1.4) 8.4(2.7) 8.0(2.2)	Suzaku RXTE RXTE RXTE Integral Integral Integral Integral Integral Integral	[enm+10a] [khdu12] [khdu12] [khdu12] [khdu12] [khdu12] [khdu12] [khdu12] [khdu12] [khdu12]
1RXS J170849.0−400910	>300 [dkh08]	… 0.86(16)	… 2.60(35)	1.46(21) 1.13(6)	5.2(1.0) [3.6(5) (20–100 keV)] 6.61(23)	Integral Integral, RXTE	[gri+07] [dkh08]
SGR J1745−2900	>50 [mgz+13]	…	…	$1.47^{+0.46}_{-0.37}$	$0.67^{+0.20}_{-0.26}$ [0.622(57) (2–79 keV)]	NuSTAR	[mgz+13]
SGR 1806−20	>160 [mhs+05]	… … … … …	… … … … …	1.9(2) 1.5(3) 1.7(1) 1.2(1) 1.6(2)	6.0(9) [4.7(5) (20–100 keV)] 11(2) [8(9) (20–100 keV)] 4.70 [$5.56^{+0.31}_{-0.23}$ (1–60 keV)] 9.89 [$5.71^{+0.65}_{-0.60}$ (1–60 keV)] 3.83 [$3.86^{+0.40}_{-0.77}$ (1–60 keV)]	Integral Integral Suzaku Suzaku Suzaku	[mgmh05] [mgmh05] [enm+10b] [enm+10b] [enm+10b]
1E 1841−045	>140 [khdc06]	0.72(15) $1.35^{+0.30}_{-0.25}$ 0.99(36)	4.00 [2.44 (10–100 keV)] 2.67 [$2.18^{+0.62}_{-0.51}$ (1–50 keV)] 3.03 [1.76(27) (3–79 keV)]	1.32(11) $1.62^{+0.21}_{-0.22}$ 1.33(3)	6.88 [5.54 (10–100 keV)] 4.59 [$4.37^{+0.39}_{-0.29}$ (1–50 keV)] 7.99 [6.84(6) (3–79 keV)]	Integral, RXTE Suzaku NuSTAR	[khdc06] [mks+10] [ahk+13]
SGR 1900+14	>100 [gmte06]	… … …	… … …	3.1(5) 1.2(5) 1.4(3)	1.6(4) [1.5(3) (20–100 keV)] 3.24 [$1.87^{+0.40}_{-0.77}$ (1–60 keV)] 1.42 [$1.07^{+0.24}_{-0.21}$ (1–60 keV)]	Integral Suzaku Suzaku	[gmte06] [enm+10b] [enm+10b]

Results

$$L_\gamma^{\rm obs} = \ 1.2 \times 10^{36}\,{\rm erg}\cdot{\rm s}^{-1}$$

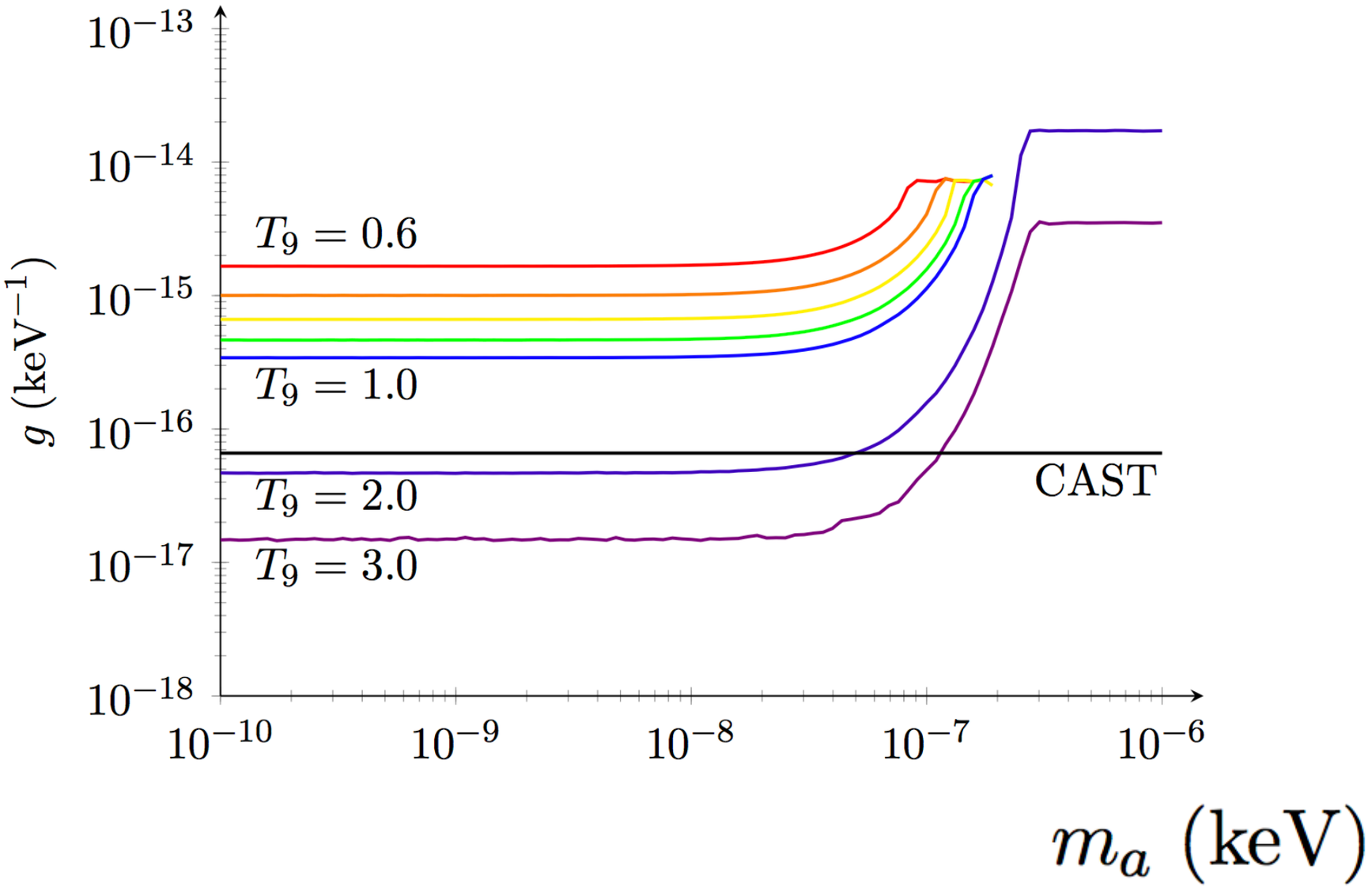

Future

polarization signals in hard X-rays

generalized initial states

spectral analysis

other signals?

generally, I expect the interface between X-ray astronomy and axion physics to be a fruitful area in the future

Plasma Effects

$$i\frac{d}{dz}\Phi = \begin{pmatrix} \omega+\Delta_a & \Delta_M & 0 \\ \Delta_M & \omega+\Delta_\parallel+\Delta_p & \sigma_{12}\omega/2 \\ 0 & \sigma_{21}\omega/2 & \omega+\sigma_{22}\omega/2 \end{pmatrix}\Phi, \qquad \Phi = \begin{pmatrix} a \\ E_\parallel \\ E_\perp \end{pmatrix}$$

$$\Delta_p \approx -\omega_{\rm pl}^2/2\omega \approx -2\times 10^{-14}\ {\rm eV}$$

$$\omega_{\rm pl}^2 = 4\pi\alpha N_e/m_e$$

$$N_e = (7\times 10^{-2}\ {\rm cm}^{-3})[B_z/(1\ {\rm G})][(1\ {\rm sec})/P]$$

$$\sigma_{11} = (q-v_e)\sin^2\theta - \frac{v_e}{1-u_e}\cos^2\theta,$$

$$\sigma_{22} = -m\sin^2\theta - \frac{v_e}{1-u_e},$$

$$\sigma_{12} = -\sigma_{21} = i\frac{v_e u_e^{1/2}}{1-u_e}\cos\theta.$$

$\Delta_p r_0 \approx$ -10

$\Delta_{\parallel 0} r_0 \approx 8.6\times 10^{13}$

plasma important at $\Delta_p \approx \Delta_\parallel$

$$\gamma_{\rm res} = \frac{4\Delta_M^2 H}{\Delta_\parallel} = 1.915\times 10^{-8}\,\frac{g_9^2 H_1}{\omega_1 \hat{q}}$$

Hard X-Ray Telescope

HXMT (20-250 keV) - 2018

Hard X-ray Modulation Telescope

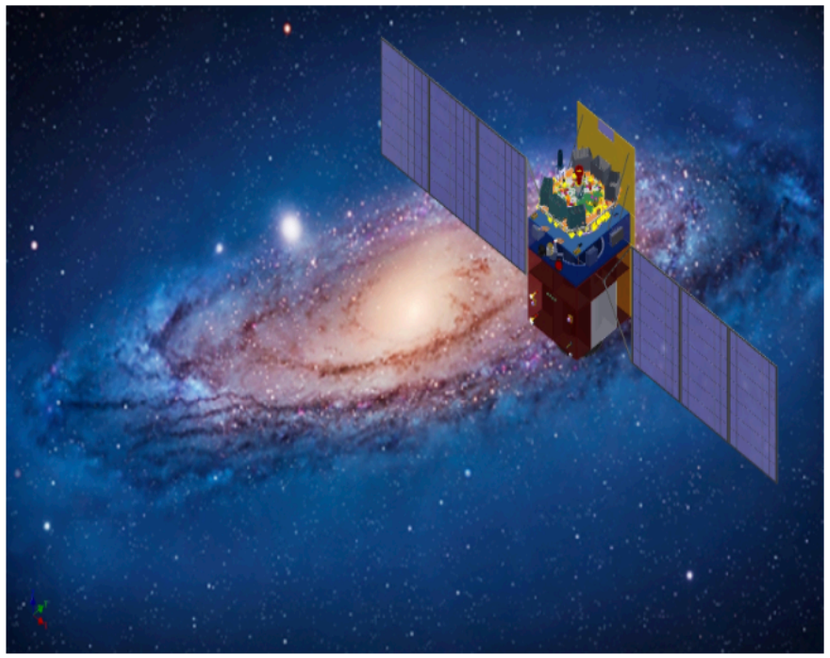

The Hard X-ray Modulation Telescope (HXMT) , named "Insight", is China's first X-ray astronomy satellite. There are three main payloads onboard Insight-HXMT, the high energy X-ray telescope (20-250 keV, 5100 cm^2), the medium energy X-ray telescope (5-30 keV, 952 cm^2), and the low energy X-ray telescope (1-15 keV, 384 cm^2). The main scientific objectives of Insight-HXMT are: (1) to scan the Galactic Plane to find new transient sources and to monitor the known variable sources, (2) to observe X-ray binaries to study the dynamics and emission mechanism in strong gravitational or magnetic fields, and (3) to find and study gamma-ray bursts with its anti-coincidence CsI detectors.

Urca Processes

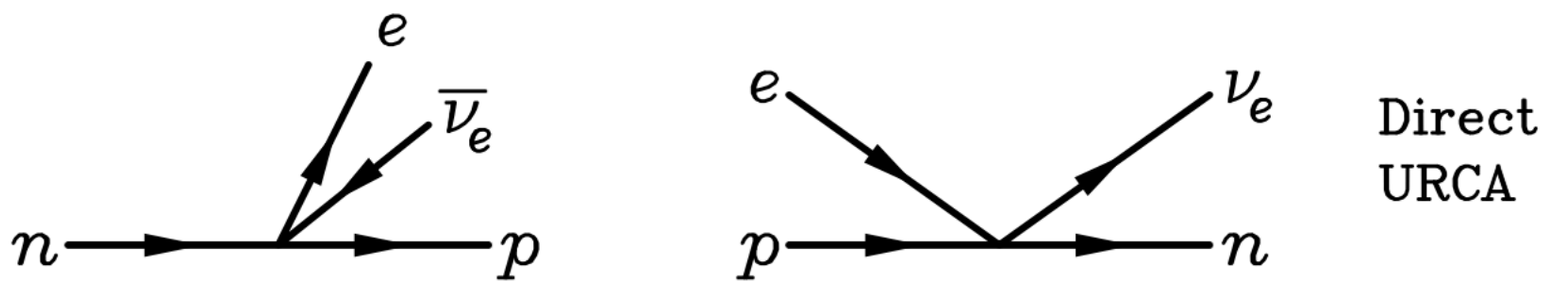

Direct URCA

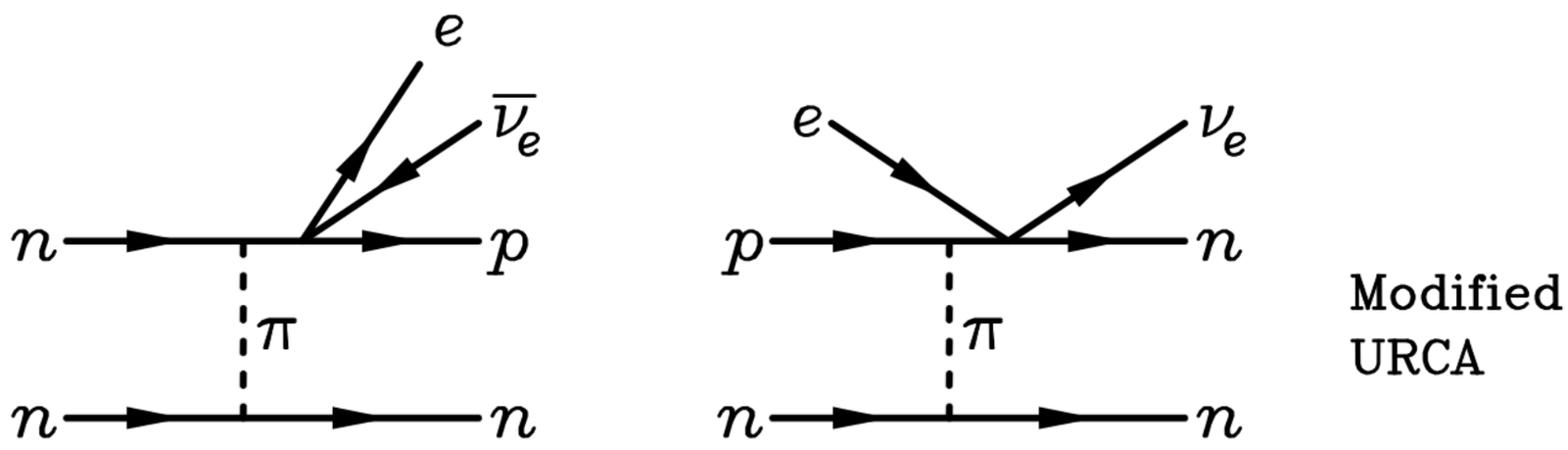

Modified URCA

Neutrino Production

$$\dot{q}_\nu^D \sim 10^{27}\, T_9^6\, \mathcal{R}_D \,\mathrm{erg\ s^{-1}\ cm^{-3}}\ (\rho \gtrsim 10^{15}\,\mathrm{g\ cm^{-3}})$$

$$\dot{q}_\nu^M \sim 7 \times 10^{20}\, T_9^8 \left(\frac{\rho}{\rho_{\mathrm{nuc}}}\right)^{2/3} \mathcal{R}_M \,\mathrm{erg\ s^{-1}\ cm^{-3}}$$

$$\dot{q}_\nu^{CP} \sim 10^{21} \left(\frac{\rho}{\rho_{\mathrm{nuc}}}\right)^{1/3} T_9^7\, f\left(\frac{T_{\mathrm{core}}}{T_{\mathrm{crit}}}\right) \mathrm{erg\ s^{-1}\ cm^{-3}}$$

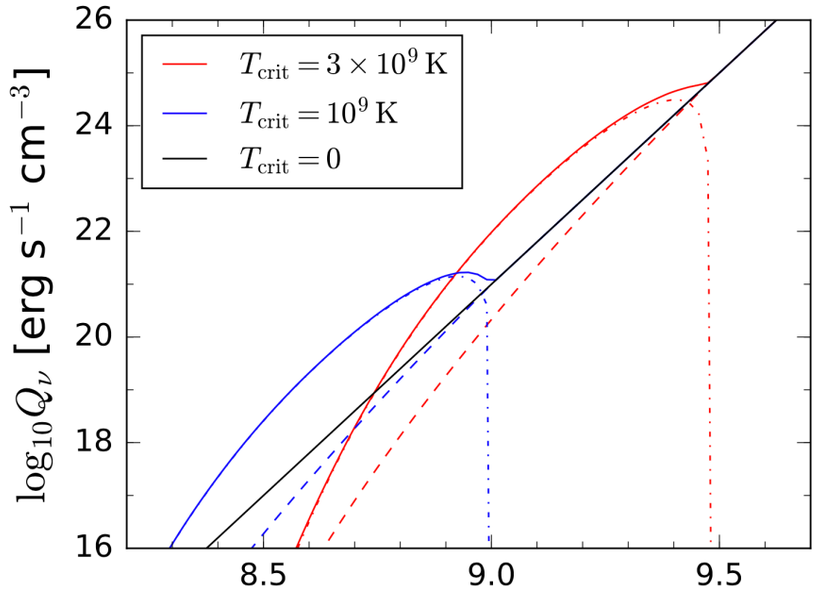

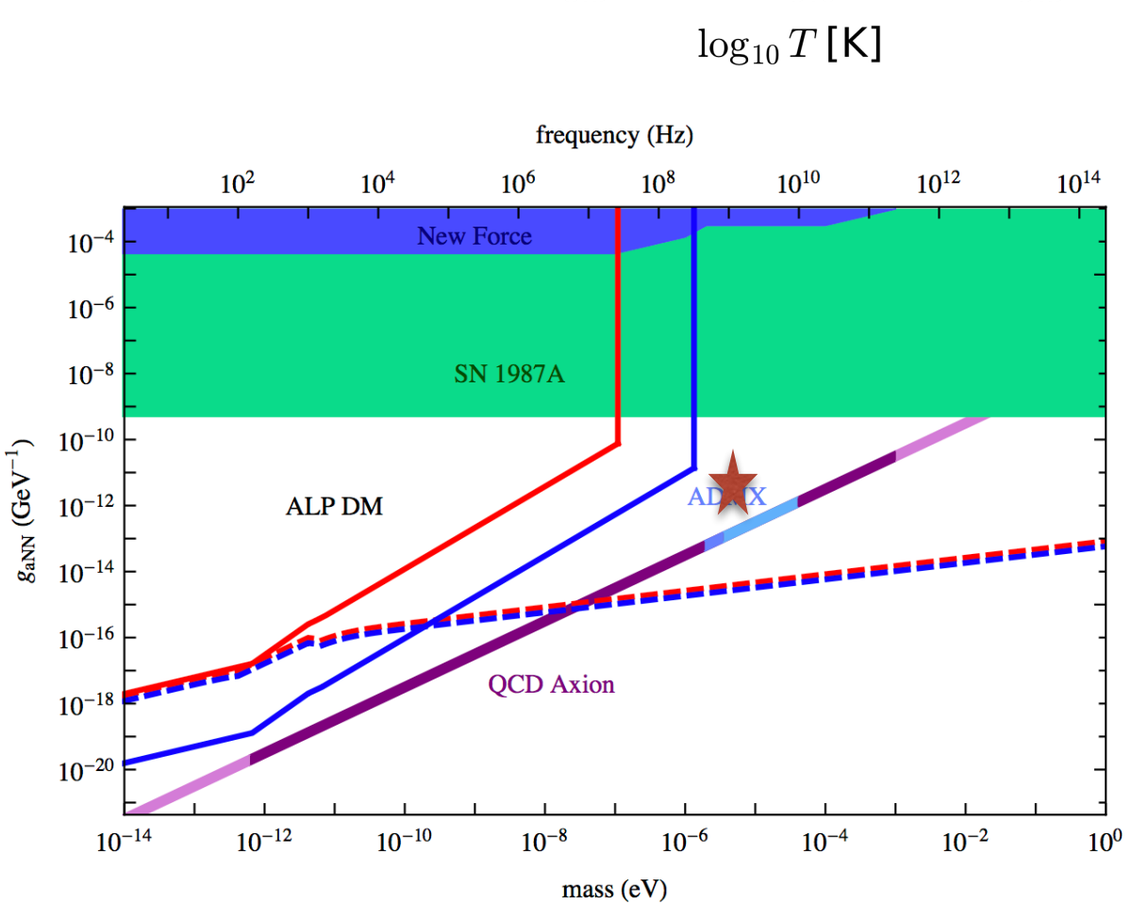

Graham et. al. (2017)

Initial Conditions

Since the focus is on the conversion probability and only the relative phase $\Delta\phi(x) = \phi_a(x) - \phi_E(x)$ appears in the equations above, one gets to

$$\begin{aligned} \frac{d\chi(x)}{dx} &= -D(x)\cos[\Delta\phi(x)], \\ \frac{d\Delta\phi(x)}{dx} &= A(x) - B(x) + 2D(x)\cot[2\chi(x)]\sin[\Delta\phi(x)], \end{aligned} \tag{2.9}$$

where $\chi(1)$ determines the initial state at the surface of the magnetar. To avoid singularities for $\chi(1) = n\pi/2$ with $n \in \mathbb{Z}$, *i.e.* for pure initial states, the initial condition for $\Delta\phi(1)$ must satisfy $\Delta\phi(1) = m\pi$ with $m \in \mathbb{Z}$. It is therefore possible to set $\Delta\phi(1) = 0$ for a pure ALP initial state[4] and the ALP-photon conversion probability is simply $P_{a\to\gamma}(x) = \sin^2[\chi(x)]$.

Magnetar Spectra

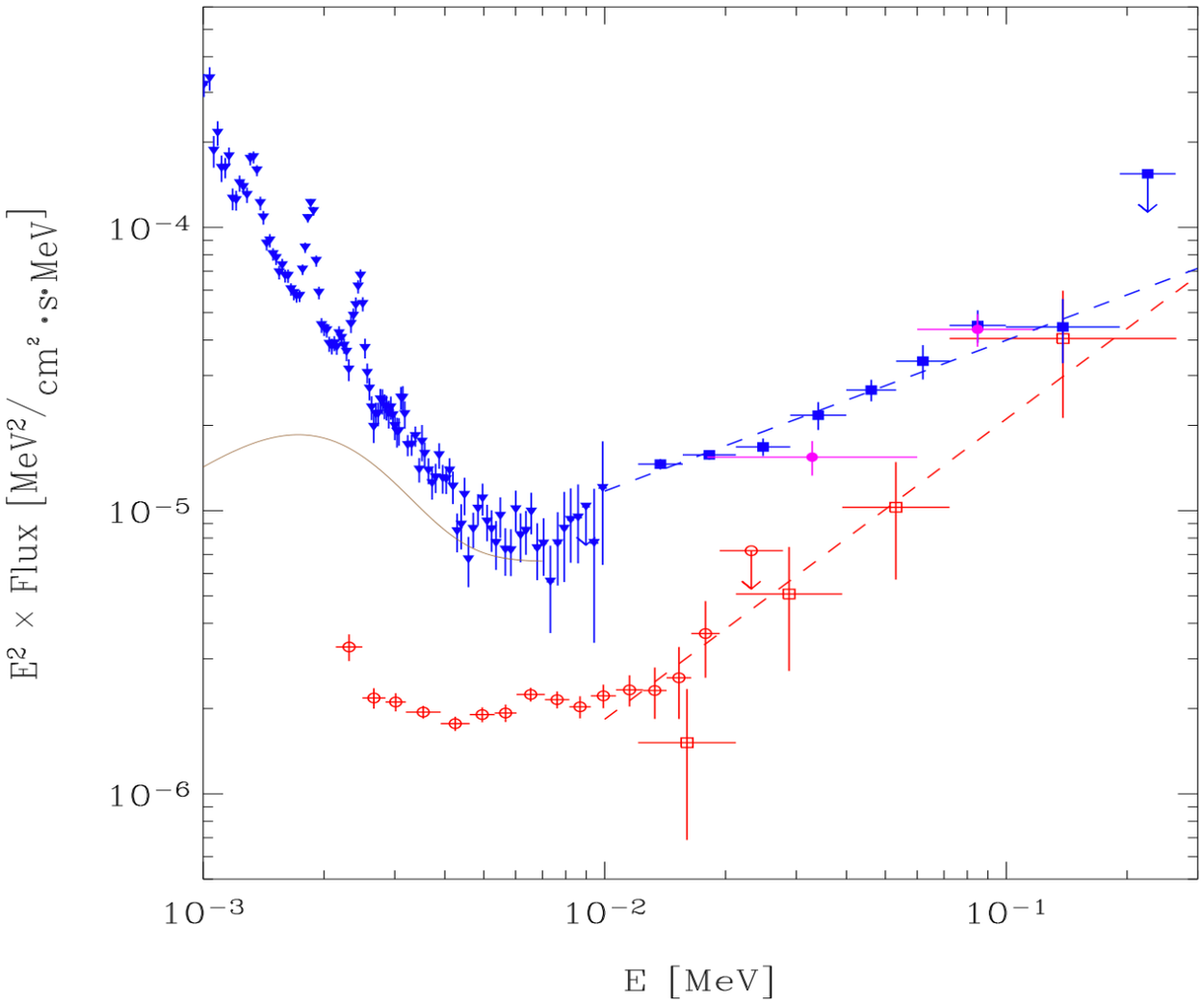

Fig. 5.— A νF_ν spectral representation of the total pulsed high-energy emission from 1E 1841-045 is shown in red (RXTE PCA; open circles, RXTE HEXTE; open squares). The total spectrum from the Kes73/1E 1841-045 complex is represented in blue (triangles; XMM EPIC PN, filled squares; RXTE HEXTE). The total (pulsed plus DC) 1-7 keV X-ray spectrum from 1E 1841-045 (Morii et al. 2003) is plotted as a solid dark orange line. The two magenta flux points are INTEGRAL IBIS ISGRI measurements given in Molkov et al. (2004). Fits (> 10 keV) to the total complex (blue) and total pulsed (red) spectra of 1E 1841-045 are drawn as dashed lines.

Kuiper et. al. (2004)

Besides spectacular outbursts, magnetars produce persistent or decaying X-ray emission with luminosity $L \sim 10^{34} - 10^{36}$ erg s^{-1}. Two peaks are observed in their X-ray spectra, with comparable luminosities. The first peak is near 1 keV; it is associated with thermal emission from the neutron star surface. The second peak is above 100 keV. Its low-energy slope (between 10 and 100 keV) was observed in 7 magnetars[1] (Kuiper et al. 2008; Enoto et al. 2010), with a typical photon index $\Gamma \sim 1 - 1.5$.

Beloborodov (2012)

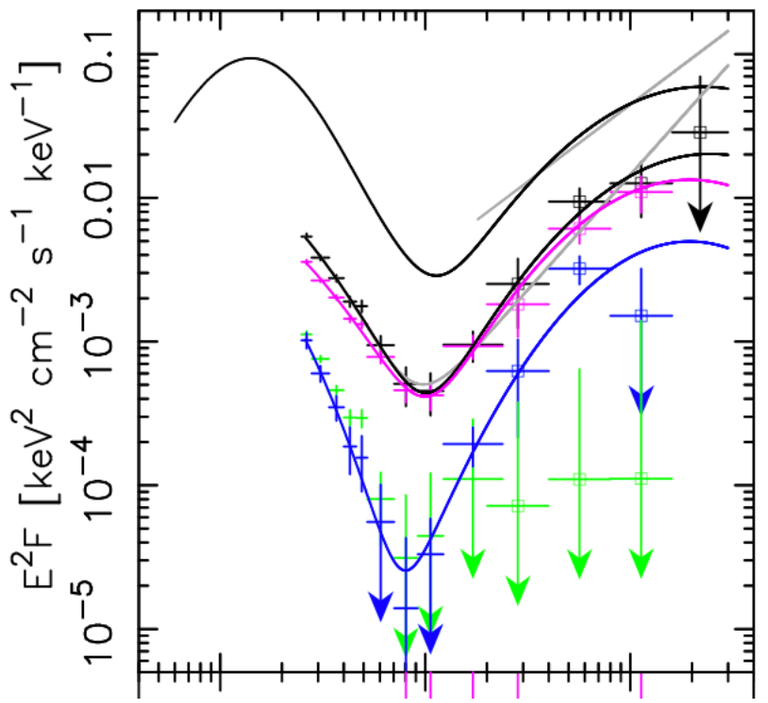

Detailed high-energy characteristics of AXP 4U 0142+61

Multi-year observations with INTEGRAL, RXTE, XMM-*Newton* and ASCA

Harotg et. al. (2008)